Materials Chemistry and Physics 255 (2020) 123600

Contents lists available at ScienceDirect

Materials Chemistry and Physics

journal homepage: www.elsevier.com/locate/matchemphys

Formation, evolution and characteristics of copper sulfide nanoparticles in the reactions of aqueous cupric and sulfide ions

Yuri Mikhlin [a,*], Vladimir Nasluzov [a], Anastasia Ivaneeva [a], Sergey Vorobyev [a], Maxim Likhatski [a], Alexander Romanchenko [a], Alexander Krylov [b], Sergey Zharkov [b,c], Debora Motta Meira [d,1]

[a] Institute of Chemistry and Chemical Technology, Krasnoyarsk Science Center of the Siberian Branch of the Russian Academy of Sciences, Akademgorodok, 50/24, Krasnoyarsk, 660036, Russia
[b] Kirensky Institute of Physics, Krasnoyarsk Science Center of the Siberian Branch of the Russian Academy of Sciences, Akademgorodok 50/38, Krasnoyarsk, 660036, Russia
[c] Siberian Federal University, Svobodny Pr. 79, Krasnoyarsk, 660041, Russia
[d] European Synchrotron Radiation Facility, 6 Rue Jules Horowitz, Grenoble, F-38042, France

HIGHLIGHTS

- $Cu_{0.7}S$ particles of 4–6 nm formed for S^{2-} to Cu^{2+} ions ratio of 2 and higher.
- Covellite-type Cu_xS NPs released S at the expense of polysulfide upon aging.
- $Cu_{2-x}S$-type NPs formed and evolved to 14 nm covellitic ones for "excess" of Cu^{2+} ions.
- NIR absorption maxima at 1100–1200 nm arose and increased upon aging.
- Polysulfide species stabilized Cu-depleted covellite and reduced the density of holes.

GRAPHICAL ABSTRACT

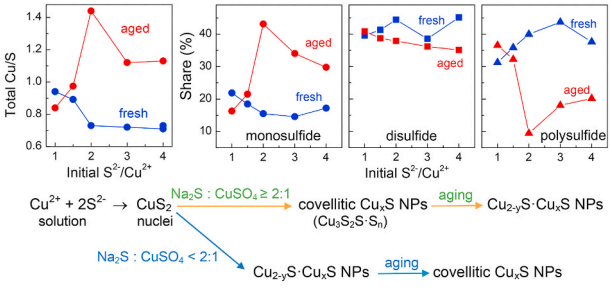

ARTICLE INFO

Keywords:
Copper sulfide nanoparticles
Polysulfide
X-ray photoelectron spectroscopy
X-ray absorption spectroscopy
DFT+*U*

ABSTRACT

Colloidal copper sulfides produced in reactions of aqueous copper and sulfide ions are important for many materials applications, environment and mineral processing. Here, Cu_xS nanoparticles formed and aged at varying copper sulfate to sodium sulfide ratios were studied using in situ UV–vis–NIR spectroscopy, dynamic light scattering, X-ray absorption spectroscopy, ex situ TEM, X-ray photoelectron spectroscopy and Raman scattering, and DFT + *U* calculations. It was established that the ratio of aqueous Cu^{2+} to S^{2-} ions of 1:2 is critical for the reaction, which yields disordered covellite-like 4–6 nm $Cu_{0.7}S$ nanoparticles comprised polysulfide species at this and higher sulfide concentrations; upon aging, the particles release sulfur and transform to chalcocite-like structure ($Cu_{2-x}S$, $x < 1$). Conversely, at the "excess" of copper ions, $Cu_{2-x}S$-type particles grew into 12–14 nm "covellitic" nanoparticles. The optical absorbance at 1100–1200 nm commonly attributed to localized surface plasmon resonance increased with time and was lowest for $Cu^{2+}/S^{2-} = 1{:}2$. DFT + *U* calculations found that polysulfide stabilizes copper-deficit covellite, while Cu vacancies in chalcocite are more favorable and

* Corresponding author.
E-mail address: yumikh@icct.ru (Y. Mikhlin).
[1] Present addresses: CLS@APS sector 20, Advanced Photon Source, Argonne National Laboratory, 9700 S. Cass Avenue, Lemont, Illinois 60439, USA; Canadian Light Source Inc., 44 Innovation Boulevard, Saskatoon, Saskatchewan S7N 2V3, Canada.

https://doi.org/10.1016/j.matchemphys.2020.123600
Received 21 May 2020; Received in revised form 29 June 2020; Accepted 23 July 2020
Available online 28 July 2020

destabilized by S–S bonding; the Fermi level energy increases and the hole density decreases with polysulfide formation. We believe that CuS_2 clusters form initially, and following conversion of disulfide to polysulfide and then monosulfide ions rather than release of Cu determines the character of Cu_xS nanoparticles.

1. Introduction

Copper sulfide nanoparticles (NPs) attract increasing attention due to unique electronic, optical and chemical properties promising for optoelectronic devices, solar cells, lithium ion batteries, nanoscale switches, sensors, photocatalysis, biomedicine and other applications [1–8]. Copper sulfides Cu_xS, $1 \leq x \leq 2$, have five stable phases at room temperature, which are typically p-type semiconductors with the band gap increasing from 1.1 eV in chalcocite (Cu_2S) to 2.0 eV in covellite (CuS), while hole densities and conductivity grow as the content of copper decreases [9–12]. In recent years, optical absorption in the near-infrared region (NIR), i.e., in the second transparency window of water and biological tissue, assigned to localized surface plasmon resonance (LSPR) have been received a great deal of attention [1–3, 13–18]. The LSPR is believed to be due to hole carriers in the valence band; it is stronger in covellite with the highest concentration of Cu vacancies and can be dynamically controlled using redox, ligand or cation-exchange reactions [19–25]. These features make copper chalcogenides prospective materials for photovoltaic and biomedical applications, and, in turn, can be used for in situ monitoring the composition and structure of copper sulfide nanoparticles and surfaces. Synthesis of copper chalcogenide nanocrystals in organic solutions allowing to control the composition, crystallinity and shape is often followed by post-synthetic treatment and transfer to aqueous solutions [1–3,16–24]. Moreover, colloidal copper sulfides of environmental concern arise in soils, waste, surface and ground waters [25–31] largely via reactions between copper cations and sulfide anions, and enter the environment from mineral processing [32–37] and nanoengineered materials [38, 39]. Nevertheless, reaction mechanisms and their relation with properties of Cu_xS NPs remain a challenge.

In the current work, we study the formation and aging of CuS colloids in the aqueous solutions containing sulfide anions and cupric cations. We examined the nanoparticle composition and structure utilizing a set of in situ and ex situ experimental techniques together with density functional theory (DFT) simulation of covellite- and chalcocite-based structures with Cu vacancies. Particularly, application of X-ray photoelectron spectroscopy (XPS) revealed changes of the nanoparticle composition and significance of polysulfide species. This allowed us to shed new light onto the mechanisms of formation, chemical behavior, and characteristics of nanoscale Cu_xS, including LSPR, and to establish that the state and reactions of sulfur rather than copper species play the major role.

2. Materials and methods

2.1. Materials and preparation

Copper sulfate ($CuSO_4 \cdot 5H_2O$) and sodium sulfide ($Na_2S \cdot 9H_2O$) were purchased from "Volzhsky Orgsynthese" (Russia); the chemicals were of analytical grade and were utilized without additional purification. The reagent solutions were prepared using deionized water (Millipore) at room temperature. In a typical procedure, copper sulfide colloids were obtained by mixing 5 mL of $CuSO_4$ solution (2 mM) and 5 mL of sodium sulfide solution whose concentration varied from 2 to 8 mM. The reaction media became brown in a few seconds; it was agitated for 5 min and then left unstirred with or without access of air. All the hydrosols were stable for 5–6 h, and coagualated in the next few hours or days depending on the composion and aging conditions. The redox potentials of the media measured using Pt wire were found to be −0.20 V, −0.29 V and −0.37 V vs. saturated Ag/AgCl reference electrode and somewhat increased with time, while pHs were of 4.8, 8.9 and 11.0 at the ratios $Cu^{2+}/S^{2-} = 1{:}1$, 1:2 and 1:3, respectively. After a predetermined time, a portion of the solution was loaded into a cell for UV–vis–NIR absorption spectroscopy, X-ray absorption spectroscopy, dynamic light scattering (DLS) or zeta potential measurements. A drop of the copper sulfide colloidal solution was placed on highly oriented pyrolytic graphite (HOPG) for XPS and Raman spectroscopy or on amorphous carbon coated Cu grid for transmission electron microscopy (TEM), and allowed to dry at ambient temperature. The dried samples were usually examined before and after cautious water rinsing to remove the solution remnants; it was established that the procedure insignificantly affected the composition of copper sulfide nanoparticles (see, for example, XPS data in paragraph 3.5).

2.2. Characterization

The optical absorption spectra were acquired in a thermostatic quartz cell (1 cm) in the wavelength range of 200–1500 nm using an UV-3600 Plus spectrophotometer (Shimadzu, Japan). Dynamic light scattering (DLS) and electrophoretic zeta potential studies were conducted with a Zetasizer Nano ZS spectrometer (Malvern Instruments Ltd, UK) at the scattering angle of 173° in a folded polystyrene cell or polycarbonate cell with Pd electrodes. The volume distributions of hydrodynamic diameter D obtained using the multiple exponential fit of correlation function are presented in the paper.

TEM imaging and selected area electron diffraction (SAED) characterization were carried out using a JEM 2100 microscope (JEOL, Japan) operated at accelerating voltage of 200 kV. X-ray powder diffraction patterns were recorded using a PANalytical X'Pert Pro diffractometer with Cu Kα radiation.

XAFS data were collected at the BM23 beamline of the European Synchrotron Radiation Facility (ESRF, Grenoble, France) operated in multibunch mode with the ring current of ~90 mA using a Si(111) double crystal monochromator and a Rh mirror with an angle of 5 mrad to reject the harmonics [40]. Cu K-edge spectra were acquired in situ from the Cu_xS hydrosols loaded into a cell with Kapton window in fluorescence mode at room temperature using a Vortex detector (Hitachi); the energy was calibrated with a Cu foil measured in transmission mode. EXAFS analysis was performed employing IFEFFIT code implemented in the Demeter package (version 0.9.25) [41]. The k^2-weighted EXAFS oscillations were treated in the photoelectron wavevector k range from 2.5 $Å^{-1}$ to 10.5 $Å^{-1}$, the forward Fourier transformed R-space data were windowed in the range of 1.0–2.236 Å. The photoelectron threshold energy E_o was first fitted from the data and then kept constant. The EXAFS signals were modelled utilizing a single path scattering approach, combining Cu–O and Cu–S paths.

X-ray photoelectron spectra were measured using a SPECS instrument equipped with a PHOIBOS 150 MCD 9 hemispherical analyzer at electron take-off angle 90° utilizing monochromatic Al Kα radiation (1486.6 eV) at room temperature. The analyzer pass energy was 10 eV for high-resolution scans and 20 eV for survey spectra. The high-resolution spectra were fitted after subtraction of Shirley-type background with Gaussian-Lorentzian peak profiles with the S $2p_{3/2,1/2}$ spin-orbit splitting of 1.19 eV and the branching ratio of 0.5, respectively, using a CasaXPS software package.

Raman spectra were collected in the backscattering geometry with a Horiba Jobin-Yvon T64000 spectrometer (Horiba, Kyoto, Japan) equipped with a liquid nitrogen cooled charge-coupled device detection system in subtractive dispersion mode. Ar^+ ion laser (Spectra-Physics Stabilite 2017) with $\lambda = 514.5$ nm and power of 1 mW on a sample was

used as an excitation light source.

2.3. DFT + U simulation

DFT calculations were performed using the GGA + U scheme [42] with PW91 parametrization of an exchange-correlation functional [43,44] and a Hubbard-type on-site U parameter as implemented in the Vienna *ab initio* simulation package (VASP) [45,46]. The U term was set to 5 eV for Cu 3d states in accordance with [47–49]. Spin unrestricted eigenfunctions of the projector augmented wave method [50,51] with explicit treatment of eleven electrons ($4s^1 3d^{10}$) for each Cu atom and six electrons ($3s^2 3p^4$) for S atoms were generated using plane waves restricted by an energy cut off of 400 eV. Numerical integration in the reciprocal space was carried out using $5 \times 5 \times 3$ and $6 \times 6 \times 6$ Monkhorst-Pack k-points grids for CuS and Cu_2S, respectively [52].

Covellite is a hexagonal crystal (space group P63/mmc) at room temperature, whose unit cell contains six formula units with the lattice constants of $a = b = 3.782$ Å and $c = 16.29$ Å [53] composed of alternating "disulfide" and "monosulfide" layers (Fig. 1), with two of three S atoms belonging to disulfide anions. Correspondingly, two out of three Cu atoms are in tetrahedral coordination and one in triangular coordination. The equilibrium lattice cell lengths calculated with $U = 5$ eV were found to be $a = b = 3.804$ Å and $c = 16.500$ Å. A $Cu_{24}S_{24}$ translation cell ($|Cu_{24}S_{24}|$) containing 24 CuS formula units with $A = B = 7.608$ Å and $C = 16.500$ Å was utilized for simulation of defect structures formed upon deletion of up to four adjacent Cu atoms. Defective configurations of Cu_2S (low chalcocite) having a cubic (anti-) fluorite structure ($a = 5.725$ Å for the cell with four formula units [10]) were calculated using $U = 5$ eV, a $Cu_{32}S_{16}$ translation cell with c axis perpendicular to (110) plane, $C = a^{U5} = 5.5644$ Å, $A = 7.869220$ Å and $B = 15.7384$ Å (consistent with the equilibrium regular lattice structure). The formation energies of defects normalized per one removed Cu atom (E^f) were calculated for arbitrary reactions of covellite and chalcocite

$$|Cu_{24}S_{24}| + n/2O_2 + nH_2O_{sol} \rightarrow |Cu_{24-n}S_{24}| + nCu(OH)_{2\ sol}, \quad (1)$$

$$|Cu_{32}S_{16}| + n/2O_2 + nH_2O_{sol} \rightarrow |Cu_{32-n}S_{16}| + nCu(OH)_{2\ sol}, \quad (1a)$$

where index 'sol' indicates solvent effect corrected total energies [54].

3. Results

3.1. Optical spectroscopy

Fig. 2 shows UV–vis–NIR absorption spectra (higher panels) of copper sulfide colloids prepared with initial molar ratios of copper sulfate to sodium sulfide (further denoted as "Cu^{2+}/S^{2-}" to differentiate from the nanoparticle composition marked as Cu_xS or Cu/S) of 1:1, 1:2, 1:3, 1:4, and then aged in sealed glassware without ingress of air. The absorbance decreased with increasing the wavelength (λ) with a minimum at 650–800 nm and then rose at higher λ showing a wide maximum at 1100–1200 nm that is commonly attributed to LSPR [13–25]. The NIR maxima increased with time, more rapidly for the solutions with higher concentrations of sulfide ions and very slowly for the system with the ratio Cu^{2+}/S^{2-} of 1:2 (Fig. 2, *a*, lower panel). It is noteworthy that the maximum did not shift despite the increase in height, in contradiction with the theory of plasmon resonance in semiconductor nanoparticles [13–17]. The band gap of Cu_xS particles can be determined from the high-frequency region of the spectra using the Tauc equation $(\alpha h\upsilon)^{1/m} = k\,(h\upsilon - E_g)$ [55], where E_g is the optical band gap, k is constant, α is absorbance, $h\upsilon$ is photon energy, and $m = 1/2$ for a direct energy gap and $m = 2$ for the indirect gap. Here, $(\alpha h\nu)^{1/2}$ was plotted versus $h\nu$ to find the indirect gap E_g (see an example in Fig. 2, *b*), which is shown in Fig. 2, *c* as a function of aging time for the media with different Cu^{2+}/S^{2-} ratios. The gaps of 1.8–1.9 eV were almost independent of the solution composition soon after the preparation but varied differently during the aging, with the E_g slowly decreased for $Cu^{2+}/S^{2-} = 1{:}2$, first increased and then decreased in case of excess of sulfide (Cu^{2+}/S^{2-} of 1:3 and 1:4), and passed a minimum at 1.5 eV for the ratio of 1:1. The higher E_g value is close to that for covellite CuS, and narrowing the band gap suggests an increasing content of Cu in Cu_xS [1–3,11–16].

The NIR maxima also grew and the band gap width decreased at all the compositions upon aging the hydrosols in air (Figs. S1 and S2, Supplementary material), with both parameters remained generally lower than those in the less oxidative conditions. Simultaneously, a considerable dissolution of copper was observed. Further, we consider the aging processes with the restricted ingress of air depicted in Fig. 2.

3.2. DLS and zeta potential

The results of dynamic light scattering and zeta-potential measurements are presented in Fig. 3. The hydrodynamic diameters of Cu_xS particles increased from ~7 to 13 nm with time for the Cu^{2+}/S^{2-} ratio of 1:1, insignificantly, from 7 to 8 nm, altered for the ratio of 1:2, and stayed about 7 nm at higher concentration of sulfide, in agreement with TEM data (see below). The respective magnitudes of negative zeta potentials very slowly changed with time near −30 mV and −45 mV, indicating rather high aggregative stability of these colloids. Nonetheless, the growth of particles at $Cu^{2+}/S^{2-} = 1$ may be related with their coalescence because the static scattering was proportional to the square of the particle size rather than the cube (not shown in Figures), suggesting that the number of nanoparticles decreased.

3.3. TEM, SAED, XRD

Representative transmission electron micrographs and particle size distributions are shown in Fig. 4 together with electron diffraction data. The nanoparticles prepared with the initial Cu^{2+}/S^{2-} ratio of 1:1 had the

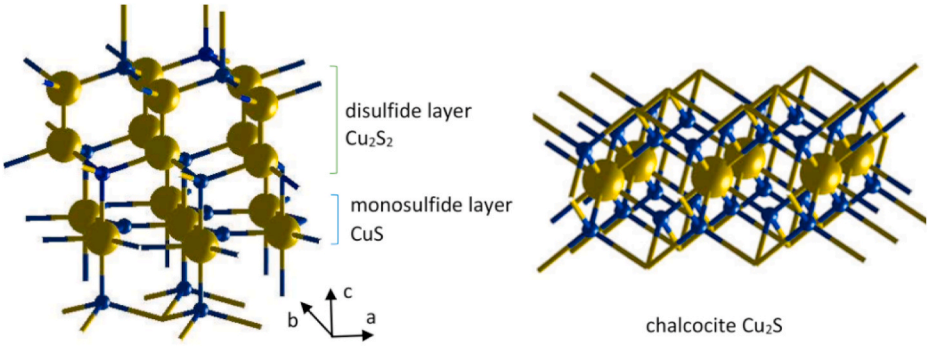

Fig. 1. Fragments of covellite (CuS) and chalcocite (Cu_2S) structures. Cu atoms are blue, and S atoms are dark yellow. (For interpretation of the references to colour in this figure legend, the reader is referred to the Web version of this article.)

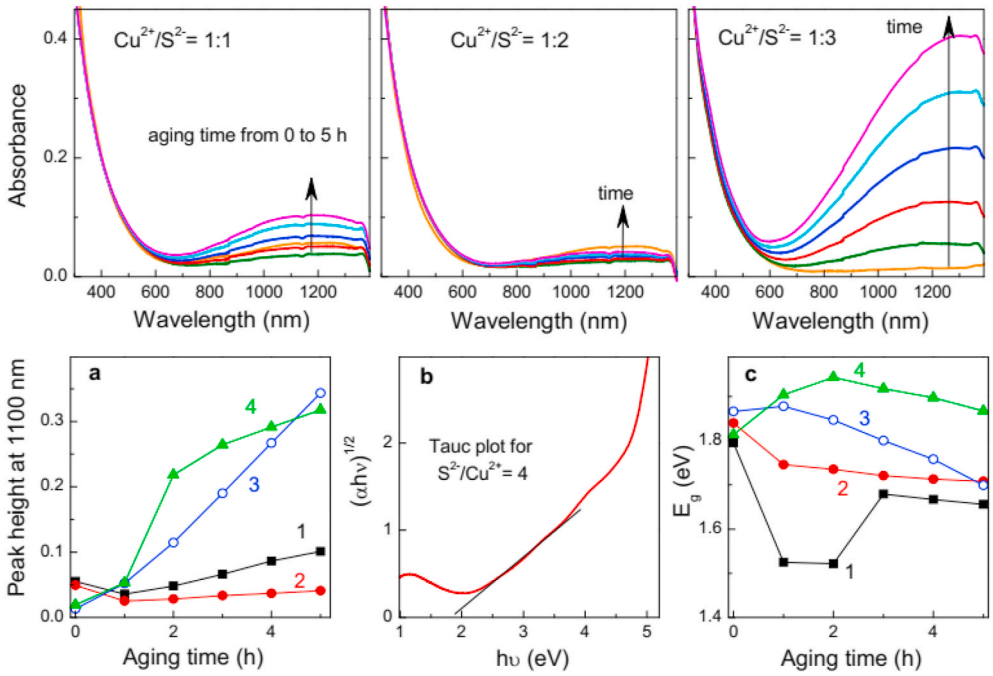

Fig. 2. UV–vis–NIR absorption spectra of the colloidal solutions of Cu_xS NPs obtained for different reaction time without ingress of air (upper panels). Lower panels: (a) optical absorbance at 1100 nm as a function of aging time; (b) an example of Tauc plot for the indirect band gap of hydrosol with Cu^{2+}/S^{2-} ratio of 1:4; (c) the band gap widths for various hydrosols as a function of aging time. The initial ratios of ions Cu^{2+}/S^{2-} were (1) 1:1, (2) 1:2, (3) 1:3, and (4) 1:4.

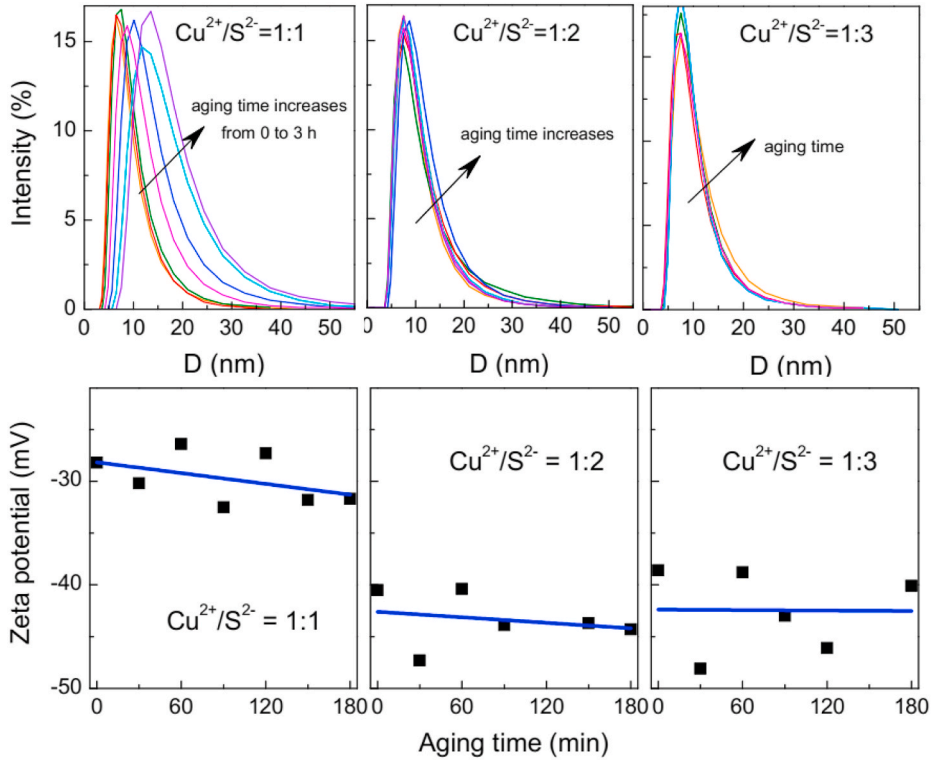

Fig. 3. Time variation of the volume distributions of hydrodynamic diameter D (upper panels) and zeta potentials (lower panels) measured for the colloids prepared using various initial Cu^{2+}/S^{2-} ratios.

diameter of ~4 nm and evolved to elongated particles of about 14 nm in the average size for the aged hydrosol. The dimensions of Cu_xS NPs produced using higher relative concentrations of sulfide ions kept the same size of about 6 nm, in good agreement with DLS data (Fig. 2). TEM images, including high-resolution TEM (Fig. S3, Supplementary material), show that smaller nanoparticles are essentially disordered while the larger ones formed and aged at the Cu^{2+}/S^{2-} ratio of 1:1 have a layered structure with the interlayer spacing of ~3 Å characteristic of covellite. Selected area electron diffraction patterns are also indicative of poor crystalline structures of the nanoparticles and suggest that

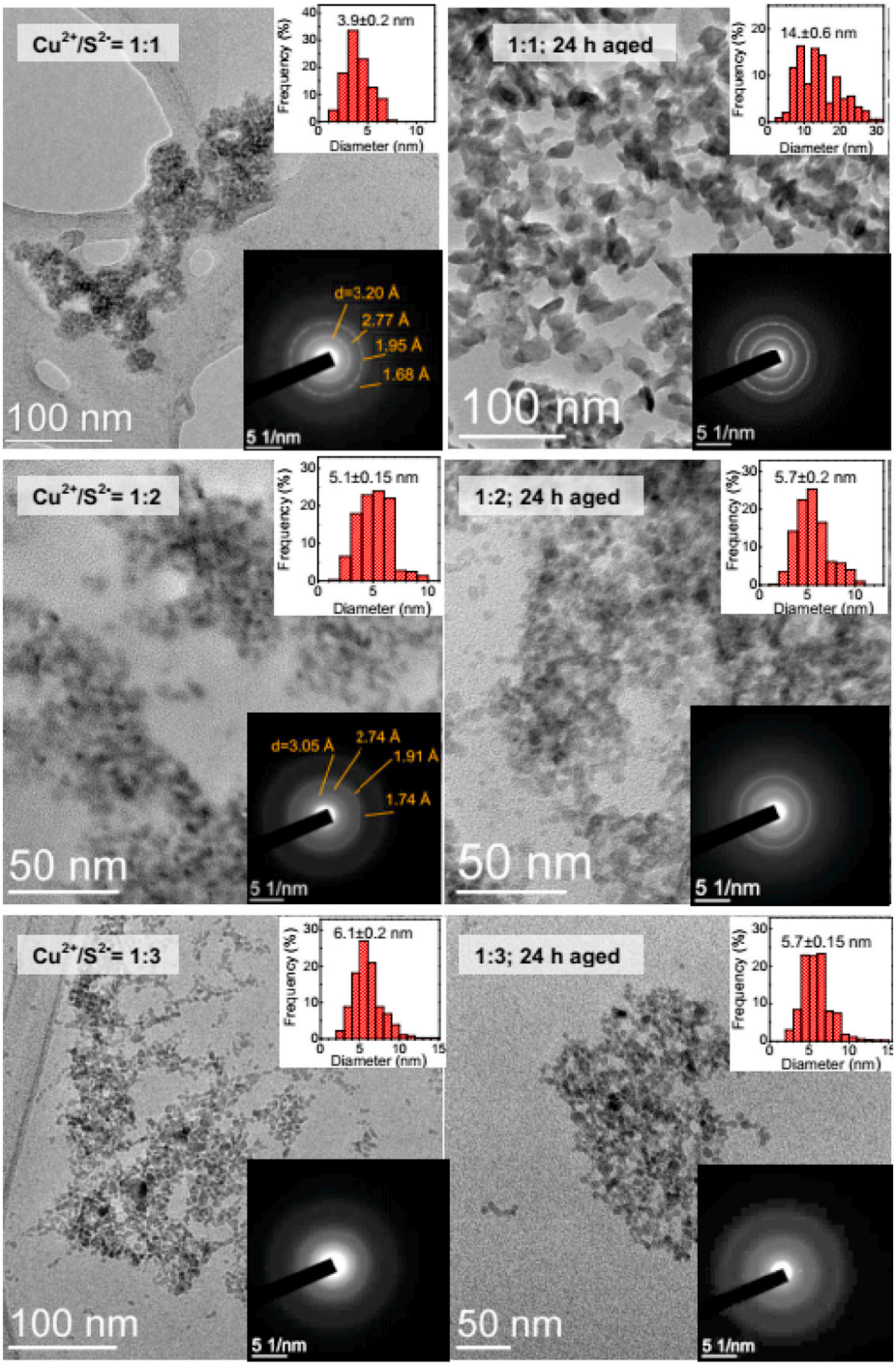

Fig. 4. TEM micrographs, electron diffraction patterns and particle size distribution diagrams of Cu_xS hydrosols prepared using various initial molar ratios of $CuSO_4$ and Na_2S. Left panels show "fresh" colloids (about 1 h after mixing the reagents), right panels show colloids aged for 24 h without air ingress.

hexagonal covellite CuS (PDF 04-004-8687) is the main product with the strongest interplane distances *d* of 3.05, 2.74 and 1.91 Å for the reaction proportion $Cu^{2+}/S^{2-} \leq 1{:}2$ and for the aged particles with the ratio of 1:1. For the particles deposited from a "fresh" sol with the proportion Cu^{2+}/S^{2-} of 1:1, the diffraction pattern with the reflections at 3.20, 2.77, 1.95 Å, etc. seems to be closer to digenite $Cu_{1.8}S$ (PDF 00-056-1256). This also agrees with X-ray diffraction data (Fig. S4), although exact speciation of essentially disordered $Cu_{2-x}S$ phases is vague. A presence of CuS_2 phase with *d* of 2.896, 2.047, 1.746 Å (PDF 04-004-6505) can be ruled out for all the colloids.

3.4. Cu K-edge XAFS

Cu K-edge XANES spectra collected from hydrosols with various proportions of copper and sulfide ions are presented in Fig. 5; the spectra of solid covellite CuS, chalcocite Cu_2S, and cuprite CuO are given for comparison. The Cu K-XANES of colloidal solutions with the initial Cu^{2+}/S^{2-} ratios ≤1:2 exhibit similar broad features at ~8990 and 9003 eV corresponding to electron transition from 1s to 4p-character states and indicative of Cu^{+}-S bonding. The spectra, however, differ from those of bulk copper sulfides CuS and Cu_2S [31,56–61], probably due to disordered structure of the copper sulfide nanoparticles. The

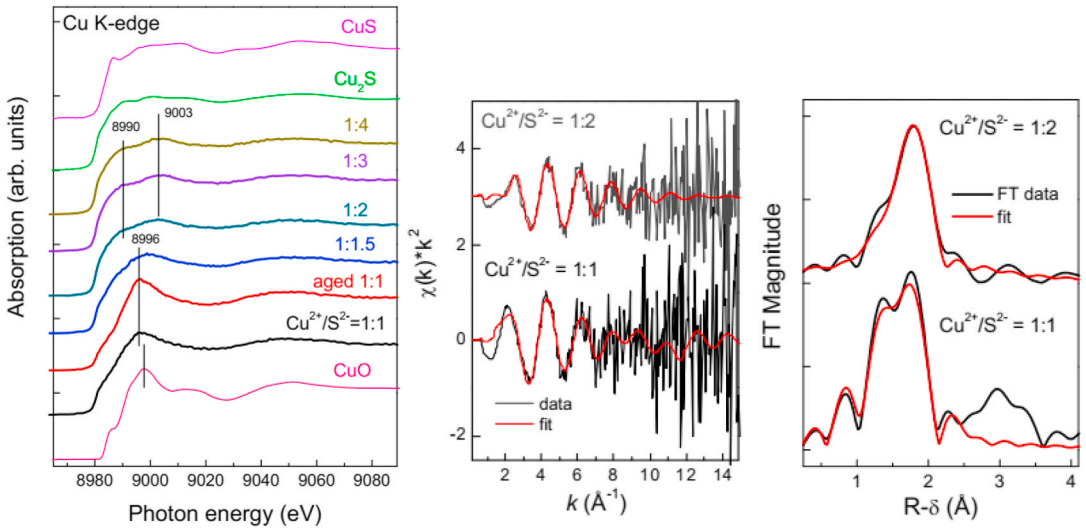

Fig. 5. Cu–K edge absorption spectra collected from hydrosols prepared with different initial Cu^{2+}/S^{2-} ratios and measured for 1 h and 7 h (sample "aged 1:1") after mixing the reagents, and the specta of solid reference compounds. Cu K-edge EXAFS results: k^2-weighted data and corresponding fits, and Fourier transforms of the k^2-weighted data and the fits of first coordination shell for "fresh" hydrosols prepared with the molar ratios Cu^{2+}/S^{2-} of 1:1 and 1:2 (right panel).

spectra collected from colloids with the Cu^{2+}/S^{2-} ratios of 1:1 and 1:1.5 showed a peak at ~8996 eV that is about 2 eV lower than the energy typical for Cu^{2+} species [58–61], for example CuO, and can be assigned to Cu^{+} ions bonded to oxygen in aqueous medium or on the particle surface. Other features are similar to those for Cu_xS phase, whose share was estimated to be ~45% before and about 55% after 7 h aging of the hydrosol with the ratio $Cu^{2+}/S^{2-} = 1:1$, and ~25% for the ratio of 1:1.5. These findings agree with negligible maxima at 8873 eV originating from transitions 1s → 3d and suggest a very low density of empty Cu 3d states.

The EXAFS results are summarized in Table 1 and also are presented in Fig. 5 for sols with the Cu^{2+}/S^{2-} of 1:1 and 1:2 as examples. Despite rather poor quality of the data collected from diluted colloidal solutions, it was possible to derive reasonable results for nearest neighbors of copper atoms (Table 1). The fitting confirmed the occurrence of Cu–O bonds of 1.9 Å for low initial sulfide concentrations ($Cu^{2+}/S^{2-} > 1:2$). There are several types of Cu and S coordination in crystalline copper sulfides [10], and the general trend is an increase of the average number of S atoms in the first coordination shell of Cu (N_S) from 3 in Cu_2S to 3.67 in CuS, while the mean Cu–S distances shorten from 2.31 Å to 2.27 Å, respectively [31]. The N_S values derived from EXAFS changed in this manner with decreasing the reaction proportion Cu^{2+}/S^{2-} but usually remained near 3 because of partial Cu–O bonding and possible effects of disordering and small particle size. The nearest-neighbor Cu–S distances ranged from 2.24 to 2.29 Å are shorter than for Cu_2S and closer to those for CuS. EXAFS analysis cannot directly resolve two Cu^{+} atoms in coordination with S^{2-} at 2.19 Å, and CuS_4 tetrahedrons with four Cu^{+} bonded disulfide anions at the Cu–S distance of 2.31 Å [10,11,31] (see Section 2.3 and Fig. 1), but variations of the coordination numbers and distances may be indicative of changes in proportions of these species [31]. In the terms used by Pattrick et al. [31], the particles examined here have "evolved" structures.

The XAFS results show, therefore, that almost all copper (I) atoms are bonded to sulfur if the Cu^{2+} to S^{2-} ratio was lower than 1:2, and some unreacted Cu^{+} ions remain in the solution at higher initial concentrations of copper.

3.5. XPS

X-ray photoelectron spectra were acquired from Cu_xS NPs after a hydrosol drop was dried on HOPG, both with and without washing to remove residual electrolyte. Before the washing, XPS found the total compositions and Cu/S ratios roughly correlated with those of aqueous media, including Na and sulfate. However, the concentration of Cu determined employing surface sensitive Cu 2p band instead of Cu 3p was about two times underestimated; minor contributions from Cu^{2+}-O species, i.e., a Cu $2p_{3/2}$ peak at the binding energy (BE) of 935 eV and shake-up satellites at 940–944 eV, were detected in the Cu 2p spectra only for the initial Cu^{2+}/S^{2-} ratio of 1:1 (Fig. 6). The contents of sulfate anions (mainly added as copper sulfate) and, in a lesser extent, disulfide anions (BE of S $2p_{3/2}$ peak of 162.7 eV) were overestimated, and their signals disappeared or notably decreased for washed samples. The facts mean that these S species were dissolved in the aqueous phase and covered the immobilized nanoparticles upon drying the hydrosols, and they were removed by water rinsing (Fig. 7). Interestingly, the intensity of sulfide components (BE of about 161.7 eV) was small even for the media with high concentrations of sodium sulfide.

We focus therefore on the photoelectron spectra from washed specimens which describe mostly Cu_xS nanoparticles (Figs. 7 and 8). The Cu 2p spectra exhibit the main Cu $2p_{3/2}$ peaks at 932.5 ± 0.1 eV while the shake-up satellites, which would originate from electron transitions to empty Cu 3d states indicating d^9 configuration in Cu^{2+} species [62–64], are absent. This is consistent with the presence of Cu^{+} ions in copper sulfides, including covellite [62]. At the same time, Cu $2p_{3/2}$ bands are

Table 1
Cu K-edge EXAFS fitting results: numbers of S and O neighbors of Cu (Ns and No), interatomic distances Cu–S and Cu–O ($R_{Cu\text{-}S}$, $R_{Cu\text{-}O}$), and corresponding Debye-Waller factors σ^2.

Ratios Cu^{2+}/S^{2-}	N_S	$R_{Cu\text{-}S}$, Å	σ^2_{Cu-S}, $Å^{-2}$	N_O	$R_{Cu\text{-}O}$, Å	σ^2_{Cu-O}, $Å^{-2}$	R-factor
1:1	1.5 ± 0.80	2.25 ± 0.02	0.003	1.30 ± 0.62	1.9 ± 0.02	0.002	0.017
1:1.5	2.41 ± 0.22	2.26 ± 0.03	0.008	0.82 ± 0.18	1.91 ± 0.03	0.003	0.0081
1:2	2.91 ± 0.33	2.24 ± 0.02	0.0085	0.12 ± 0.38	1.89 ± 0.02	0.005	0.0069
1:3	2.9 ± 0.35	2.29 ± 0.03	0.008	–		–	0.015
1:4	3.38 ± 0.61	2.27 ± 0.02	0.0108	–	–	–	0.034

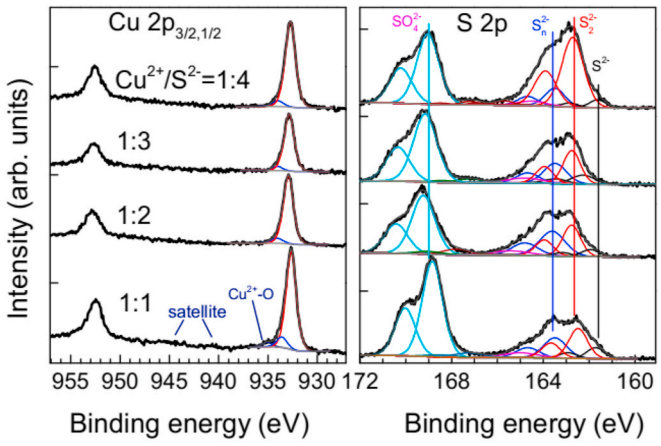

Fig. 6. Cu 2p and S 2p X-ray photoelectron spectra acquired from fresh copper sulfide hydrosols prepared with various ratios Cu^{2+}/S^{2-} and dried on HOPG (no washing).

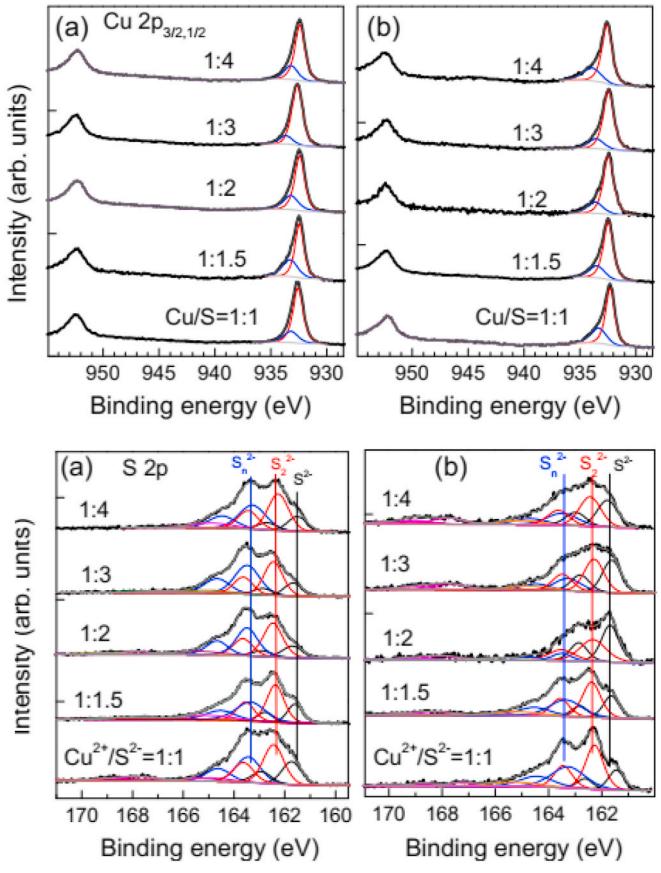

Fig. 7. X-ray photoelectron Cu 2p (upper panels) and S 2p spectra acquired from (a) fresh and (b) 24 h aged copper sulfide NPs prepared with various molar ratio Cu^{2+}/S^{2-}, dried on HOPG and washed with water.

better fitted using an additional maximum at ~933.5 eV with the relative intensity of 12–15% and a minor one at ~934.5 eV of less than 3–5% for "fresh" samples. The last component may be assigned to Cu atoms bonded to oxygen on the surface of Cu_xS nanoparticles and/or to copper hydroxides precipitated from the solutions, as its intensity normally correlates with the intensity of hydroxide in O 1s spectra at ~531.3 eV (not in Figures). The line at 933.5 eV can be attributed to "shake-off" satellites, which are due to electron transitions to unoccupied states above the Fermi level in the upper valence band composed of Cu 3d - S sp states (see below Figs. 10 and 11 and refs. [49,65,66]). The intensities of these features (Fig. S5, Supplementary material) somewhat increased for the aged media with the ratio $Cu^{2+}/S^{2-} > 1:2$; however, we refrain from making conclusions since the lines are not well resolved and their fitting is not unambiguous.

The S 2p spectra can be fitted using three doublets with the S $2p_{3/2}$ peaks at about 161.5 eV, 162.4, and 163.5 eV attributable to mono-, di-, and polysulfide anions, respectively, and a broad satellite at ~165 eV [62,67–69]. The higher binding energy components from S–O compounds (sulfate, thiosulfate, sulfite) were insignificant and only slightly increased for the aged hydrosols.

It is most important that the monosulfide components increased and polysulfide ones decreased upon aging the hydrosols with initial proportion $Cu^{2+}/S^{2-} \leq 1:2$, and changed in the opposite direction for the $Cu^{2+}/S^{2-} = 1:1$. Fig. 8 shows that the total composition of nanoparticles immobilized from "fresh" sols was close to CuS only for the lowest initial concentration of sulfide, and the atomic Cu/S ratio approached ~0.7 ($Cu_{0.7}S$) for the higher contents of aqueous sulfide in the reaction media. The relative concentrations of disulfide (about 40%) and monosulfide (15–20%) somewhat differ from that in covellite having the proportion of the relevant S 2p lines of 2:1. The high concentration of polysulfide species may be due to post-synthetic surface oxidation of Cu_xS NPs but it seems more likely that S_n groups are constituents of the nanoparticles. This concurs with the fact that the compositions determined using Cu 2p line and Cu 3p line (with a larger probing depth) differ insignificantly for the washed "fresh" samples.

The copper content in the nanoparticles drastically increases after the aging, passing the maximum of $Cu_{1.4}S$ at the reaction ratio Cu^{2+}/S^{2-} of 1:2. The difference arising between the compositions calculated using Cu 2p and Cu 3p bands suggests that the particle surface is now enriched in copper relative to the core. The concentrations of sulfur decreased mainly at the expense of polysulfide species while the share of monosulfide enhanced, again with an extremal point at the initial proportion Cu^{2+}/S^{2-} of 1:2. The relative concentrations of disulfide insignificantly reduced, and minor S–O components arose. On contrary, the total content of sulfur and the share of polysulfide increased upon aging the colloids with the initial ratio Cu^{2+}/S^{2-} of 1:1. Therefore, "covellitic" nanoparticles lost up to a half of sulfur, mainly from polysulfide, and partially transformed to chalcocite- or digenite-like $Cu_{2-x}S$ structures with $x < 1$. The opposite occurred in the solution with "excessive" copper ions, accompanied by the particle growth (Figs. 3 and 4).

3.6. Raman spectroscopy

The Raman spectra (Fig. 9) display the features at 473 cm^{-1} due to A1g LO mode vibrations (S–S stretching) and 264 cm^{-1} (lattice mode A1g TO), both of which are characteristic of hexagonal covellite and inactive in copper-enriched sulfides [70,71]. Their intensities agree with the quantities of covellite-like structure derived from other methods, being the lowest for the medium with the reaction composition Cu^{2+}/S^{2-} of 1:1. After aging, the largest amount of covellite was observed for the ratio Cu^{2+}/S^{2-} of 1:1, and the smallest was for the "stoichiometric" ratio of 1:2, in accord with the XPS data. The spectra of the aged particles also revealed a feature at 408-415 cm^{-1} that has been found, in particular, for "as deposited" CuS thin film, disappeared after annealing, and was tentatively attributed to an amorphous non-stoichiometric sulfur-enriched "covellitic" phase [70]. The current results suggest that such a phase is rather copper-enriched.

3.7. DFT + U

The DFT + *U* study was focused on highly-defective structures having a composition that can be considered as Cu-depleted covellite Cu_xS, $x < 1$, or chalcocite $Cu_{2-x}S$, $x > 1$. Fig. 10 shows low-energy configurations found for the translation cell $Cu_{24}S_{24}$ containing copper vacancies and additional S–S bonds; their energies per one removed Cu atom were

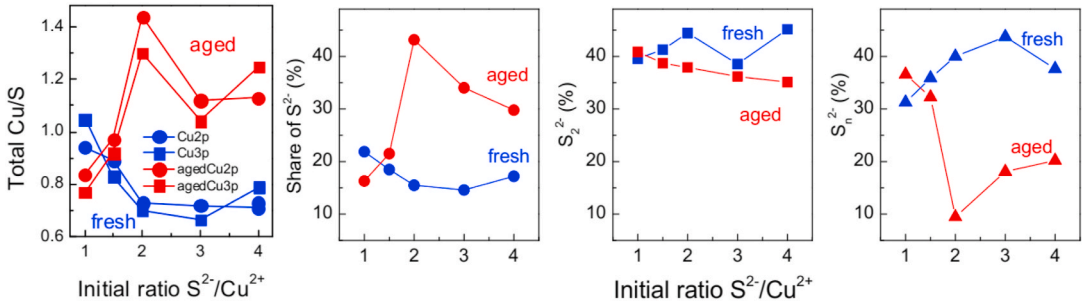

Fig. 8. Atomic Cu/S ratios (left panel) and the proportions of mono-, di- and polysulfide components determined using XPS for copper sulfide NPs prepared with various initial ratios S^{2-}/Cu^{2+}, dried and washed on HOPG. "Fresh" nanoparticles and "aged" ones were immobilized and studied in about 1 h and 24 h after mixing the reagents, respectively. Contents of copper were determined using Cu $2p_{3/2}$ (circles) or Cu 3p (squares) bands having lower and higher probing depths.

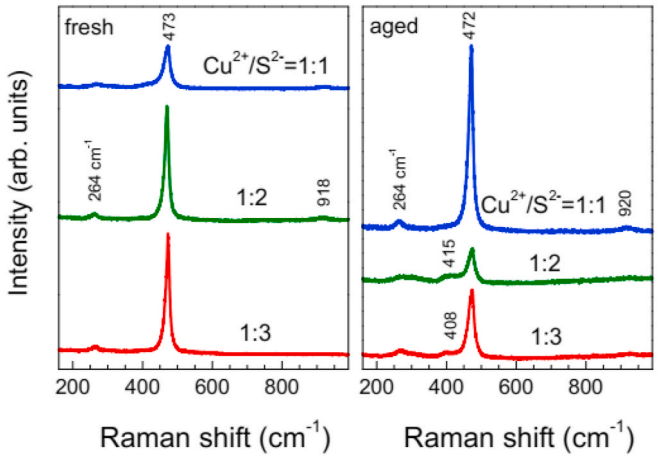

Fig. 9. Raman spectra of copper sulfide nanoparticles prepared using different ratios Cu^{2+}/S^{2-}, dried and washed on HOPG. "Fresh" hydrosols were studied in about 1 h and "aged" ones in 24 h after mixing the reagents.

calculated relative to the arbitrary reaction (1). The S–S bond in S_2 group in regular crystal is calculated to be 2.09 Å. The Cu–S bonds in the first coordination sphere of the S_2 anions are of 2.32 Å, and the ones in the plane containing three-fold coordinated Cu and five-fold coordinated S anions (Cu^{3c}-S^{5c} bonds) are of 2.20 Å, whereas the Cu^{4c}-S^{5c} bonds are the longest (2.35 Å). More details on coordination in the defect centers are given in Table S1 (Supplementary material). The lowest formation energy per Cu vacancy E^f of 1.00 eV was found for the center **1**-4VS_4 incorporating four Cu vacancies and one S_4 group in the monosulfide layer. The defect configurations with 2 and 3 vacancies of Cu and di- and trisulfide groups in this layer are by about 0.2 eV per Cu vacancy less favorable. Cu vacancies in disulfide layer of covellite are less stable, although the structure **4** with four deleted Cu atoms and disulfide anions transformed to two S_4 groups has about the same E^f. Interestingly, the formation of Cu vacancies without additional S–S bonding in both layers (structures **5**–**7** and **9**), as well as $S_3 + S_5$ groups and other configurations require higher energies. Furthermore, breakage of S–S bonds in disulfide anions is very unfavorable.

The density of states (DOS) of intrinsic and Cu-depleted covellites (Fig. 10, right panel) show that the upper part of the valence band (VB) is mainly composed of Cu 3d and S 3sp states with the Fermi level (E_F) laying below the VB top, in agreement with the results reported previously [1–3,57]. As a first approximation, DOS insignificantly varied for different defective structures, and the energy E_F, which was lowest for stoichiometric covellite, slightly shifted towards the valence band edge as Cu vacancies emerged. At the same time, the formation of polysulfide groups increased the Fermi level energies by 0.2–0.5 eV, and so substantially reduced the density of holes. These tendencies are more expressed for Cu vacancies and S–S bonding in monosulfide layer than in disulfide layer of covellite.

The DFT + U simulation of Cu-depleted chalcocite (Fig. 11, see also Table S2) revealed that configurations with Cu vacancies are about 1.2 eV more favorable than the most stable Cu-deficient structures of covellite. The defects without S–S bonding arose easier than those with disulfide anions, and additional S–S bonding to polysulfide was highly unfavorable. The Fermi level situated in the band gap for intrinsic chalcocite shifted by 0.5–0.6 eV below the valence band top as Cu vacancies emerged, and insignificantly changed for different defect configurations. However, the energy E_F increased if disulfide anions formed, e.g. in configuration **9**.

4. Discussion

4.1. Reactions of Cu_xS nanoparticle formation and evolution

The data of various techniques suggest that the initial ratio Cu^{2+}/S^{2-} of 1:2 corresponds to a special point in the reaction stoichiometry, producing mainly covellite-like phase despite of the covellite formula $Cu^{+}{}_3(S_2)^{2-}S^{2-}$ with the ratio Cu/S of 1:1. This can be interpreted in terms of initial oxidation of sulfide to disulfide anions by cupric ions (and possibly oxygen)

$$nCu^{2+} + 2\,nS^{2-} \rightarrow n[Cu^{+}S_2^{2-}]^{-} + ne^{-}, \quad (2)$$

followed by nucleation of Cu(I) disulfide clusters, probably resembling "disulfide" layers in covellite but incorporating also copper vacancies (see structure **7** in Fig. 10 as an example). In fact, the particles examined soon after the synthesis had the composition close to $Cu_{0.7}S$, and contained monosulfide and polysulfide species in addition to disulfide. We suggest that the initial product further transforms to Cu-depleted covellite-like phase via disproportionation of disulfide anions to polysulfide and monosulfide species:

$$S_2^{2-} + 2/n\,e^{-} \rightarrow S^{2-} + 1/n\,S_n^{2-}, \text{ or}$$

$$n[Cu^{+}S_2^{2-}]^{-} + ne^{-} \rightarrow n/3[Cu_3^{+}S_2^{2-}\cdot S^{2-}]\cdot S_n^{2-}. \quad (3)$$

The above results imply that polysulfide is associated with quasi-bulk structures similar to those depicted in Fig. 10 (e.g., configurations **1**–**4**). Both the experimental and theoretical findings indicate that a direct split of disulfide anions yielding monosulfide anions is unlikely, so the reaction seems to proceed via the formation of intermediary polysulfide, which then detaches monosulfide anions.

Subsequent slower aging of covellite-like nanoparticles in slightly oxidizing environment causes further decrease of the sulfur content at the expense of polysulfide and, in a lesser extent, disulfide anions via an arbitrary reaction

$$S_n^{2-} + 0.5x\,O_2 \rightarrow (n\text{-}1)S^{2-} + SO_x^{2-},\ n \geq 2. \quad (4)$$

The dimensions of the nanoparticles altered insignificantly, so the

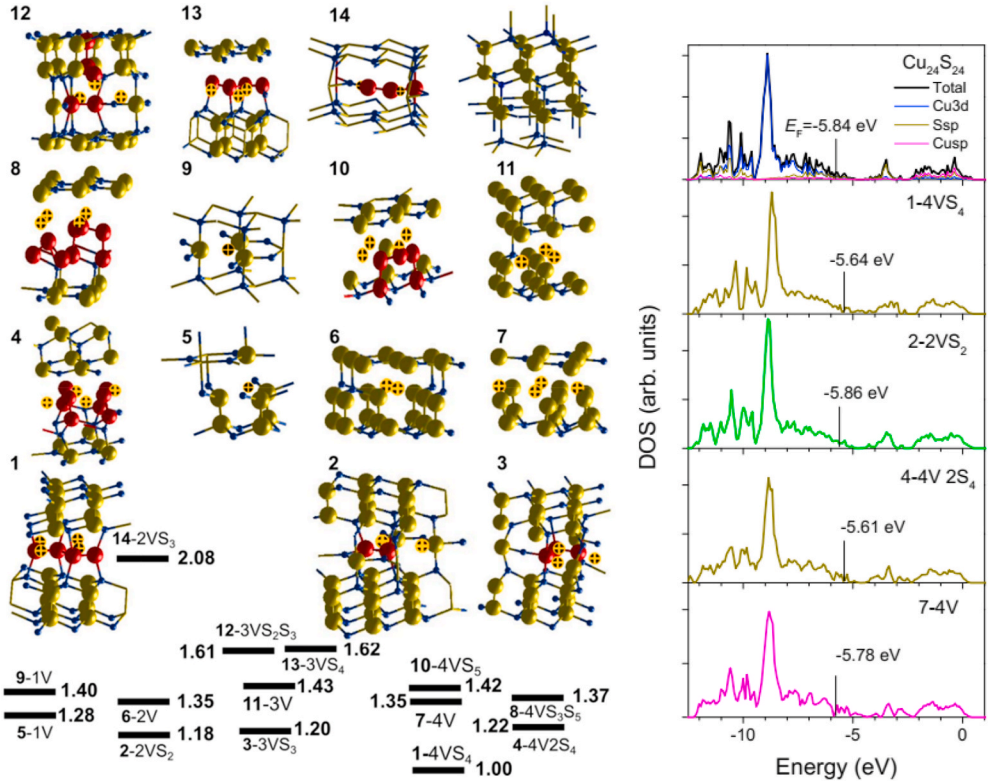

Fig. 10. Selected defect centers in covellite containing Cu vacancies, their formation energies per one removed Cu atom and total DOS distributions (partial DOS are also shown for initial CuS). Copper atoms are blue, Cu vacancies are marked with a cross, sulfur atoms are dark yellow or red (in arising S–S species). The centers, for example **1**-4VS$_4$, are denoted with an index number (**1**), amount of deleted Cu atoms and vacancies formed (4 V), a sort and number of polysulfide group formed (S$_4$), and formation energy per Cu vacancy (1.00 eV). The Fermi level energies (E_F) are indicated at DOS plots. (For interpretation of the references to colour in this figure legend, the reader is referred to the Web version of this article.)

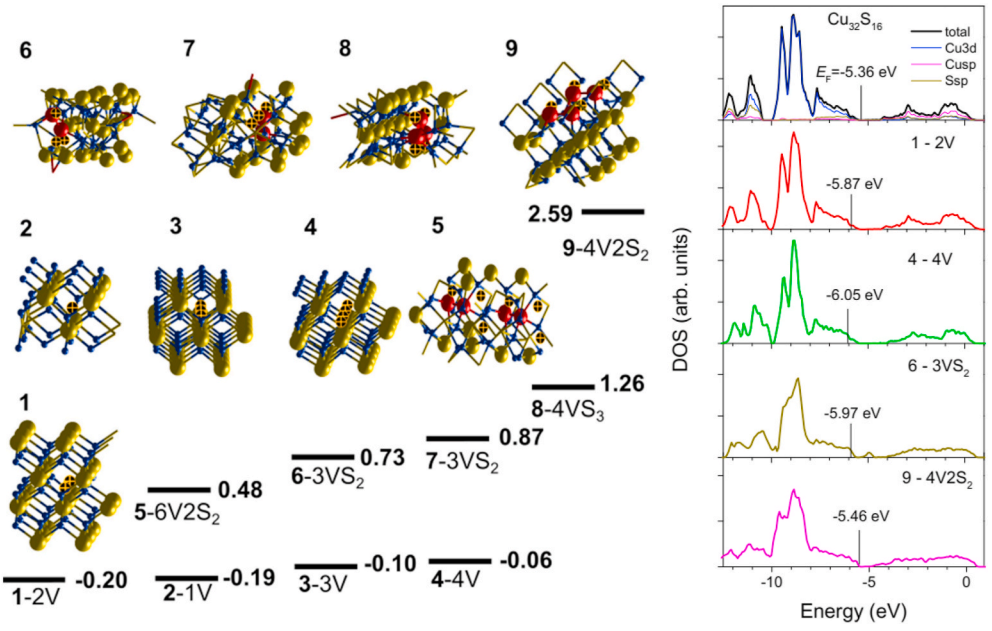

Fig. 11. Selected defect centers, formation energies per one removed Cu atom and total DOS in Cu-depleted chalcocite. Copper atoms are blue, Cu vacancies are marked with a cross, sulfur atoms are dark yellow, or red in S–S species. The centers, for example **9**-4V2S$_2$, are denoted with an index (**9**), amount of deleted Cu atoms and vacancies arisen (4 V), quantity (2) and a sort of S–S group formed (S$_2$), and formation energy per Cu vacancy (2.59 eV). The Fermi level energies (E_F) are indicated at DOS plots. (For interpretation of the references to colour in this figure legend, the reader is referred to the Web version of this article.)

transformation between Cu$_x$S and Cu$_{2-x}$S structures mainly occurred in the solid state. It is interesting that polysulfide was mostly removed and the content of covellite became minimal for the aged nanoparticles in the medium with the initial "stoichiometric" ratio $Cu^{2+}/S^{2-} = 1{:}2$. So, excessive aqueous sulfide and disulfide ions seemed to stabilize both the polysulfide and covellite, maybe, simply reducing the electrochemical potential of the dispersion.

The behavior of colloids formed at the initial ratios Cu^{2+}/S^{2-} of 1:1 and 1:1.5 is different. The particles of the composition close to CuS appear to form via the reactions (2) and (3), but some "excessive" cuprous ions remain in the solution. The nanoparticles contain more monosulfide anions but still >30% of S as polysulfide; the share of covellitic structure is smaller. Upon aging, the quantity of aqueous Cu–O species as well as the total content of S in the nanoparticles increased, and the particles grew. This means that the production of covellite-like phase involves a release of cuprous ions, as it is accepted for oxidation of Cu$_{2-x}$S nanoparticles [1–3,16–25], and particle growth, probably through the coalescence mediated by copper cations.

Previously, Pattrick et al. [31] have suggested two mechanisms for ordering the amorphous CuS precipitate started either from

wurtzite-type CuS clusters transformed then into covellitic structures containing disulfide anions, or from trigonal layers Cu_3S–CuS_3 with disulfide anions, with perhaps the incorporation of H. The latter resembles the reaction pathway proposed in this research for the formation of nanoscale Cu_xS, which, however, takes into consideration the substantial excess of S and polysulfide species. Also, minor or no attention has been paid to the Cu^{2+} to S^{2-} proportion in the reaction media [31]. The current results demonstrated that the ratio of copper ions to sulfide ions largely controls the formation, characteristics and aging behavior of Cu_xS nanoparticles.

4.2. Electronic structure and NIR absorption

There exists some controversy in the literature about oxidation state of Cu in covellite, since the formula $(Cu^{+})_3S_2^2$–S^{2-}·means an excessive electron, which should be neutralized [1–3,49,65,66,71–73]. It has been proposed that a hole is localized at sulfide anions [53], disulfide group [73], or Cu has actually the oxidation state higher than +1 [58,72]. For instance, Kumar et al. [58] have proposed the ionic model $(Cu_{Td})^{+}(Cu_T)^{+}(Cu_{Td})^{2+}(S_2)^{2-}(S)^{2-}$, where Cu_{Td} and Cu_T are tetrahedral and trigonal copper sites, respectively.

The negligible intensities of shake-up satellites in the photoelectron Cu 2p spectra at 940–944 eV (Figs. 7 and 8), which are a signature of $3d^9$ configuration, imply an absence of holes localized in the Cu 3d band and Cu^{2+} cations. At the same time, broadening the band Cu $2p_{3/2}$ at higher binding energies attributable to shake-off satellites, and the satellite at ~164.5–165 eV in S 2p spectra indicate that free holes can be delocalized just above the Fermi level at the vacant Cu 3d states hybridized with S s,p states (see also [49,65,66,72]), thus providing the positive charge necessary for charge balance.

Free holes are widely believed to determine the surface plasmon resonance peak, whose position in the near-infrared spectral region corresponds to the hole concentration of approximately 4×10^{21} cm^{-3} [12–23,74]. Both frequency and intensity of LSPR are expected to increase as a square root of the carrier density, which is due to copper vacancies and increases with oxidation of $Cu_{2-x}S$ nanoparticle due to release of copper and the transformation toward CuS. We observed here the growth of optical absorbance with sol aging and a rough correlation of the NIR peak with the content of covellite-like structure. At the same time, the DFT + *U* calculations revealed the Fermi level shifts in various defective structures, particularly due to the formation of polysulfide (Figs. 10 and 11) reducing the hole density. The lowest absorbance was, however, observed for the "stoichiometric" reaction ratio Cu^{2+}/S^{2-} of 1:2, when the amounts both of covellitic structure and polysulfide species in the aged nanoparticles were minimal. Also, the changes of NIR intensity had almost no effect on the maximum position, in contradiction with the theory [13–17]. These facts suggest a complicated mechanism of the NIR absorbance that may even be different than the localized surface plasmon resonance and requires further exploration.

5. Conclusions

In situ UV–vis–NIR spectroscopy, DLS, zeta-potential measurement, XAS and ex situ TEM, electron and X-ray diffraction, XPS, Raman scattering revealed that the reaction ratio of aqueous copper ions and sulfide ions of 1:2 is a critical, "stoichiometric" composition for spontaneously formed copper sulfide hydrosols. The nanoparticles produced with that and higher relative concentrations of sulfide ions had stable size of 4–6 nm and zeta potentials of −40 mV to −50 mV. The Cu_xS, x~0.7, nanoparticles were composed of disordered phase close to covellite and contained excessive sulfur as polysulfide species. During aging, the "covellitic" nanoparticles released sulfur, mainly at the expense of polysulfide, and transformed to the ones with composition $Cu_{2-x}S$, $x < 1$, and partial chalcocite- or digenite-like structures. In opposite, about 6 nm particles of largely $Cu_{2-x}S$ type evolved to 12–14 nm covellite-like nanoparticles in the sols with "excessive" copper ions which remained in the solution. The NIR absorption maxima at 1100–1200 nm considerably increased over aging of all the colloids, with the intensity roughly correlated with the content of covellite that was lowest for the "stoichiometric" reaction ratio Cu^{2+}/S^{2-} = 1:2. DFT + *U* simulation found that the copper-depleted structures of covellite were stabilized by polysulfide species; direct splitting of disulfide groups to monosulfide anions was unfavorable. The Fermi level located within the valence band and shifted towards the band edge so the density of free holes decreased with the formation of polysulfide. In Cu-depleted chalcocite $Cu_{2-x}S$, Cu vacancy configurations without S–S bonding formed easier than those with disulfide and especially polysulfide anions. We hypothesize that clusters CuS_2 similar to the disulfide layers in covellite but depleted in copper arise due to the initial reduction of Cu^{2+} to Cu^{+} and oxidation of sulfide to disulfide anions. The clusters convert to the Cu_xS nanoparticles and then $Cu_{2-x}S$ phases via transformation of disulfide groups to monosulfide with polysulfide species as intermediates. The NIR absorbance depends on the composition and defectness of copper sulfide nanoparticles, particularly on the content of polysulfide, in a complicated manner differing from that expected for LSPR. The novel mechanisms of formation and conversion of copper sulfide nanoparticles underline the role of sulfur species; this is important for understanding the structure and properties of copper sulfide nanoparticles in materials science and applications, and behavior in the natural environment.

CRediT authorship contribution statement

Yuri Mikhlin: Conceptualization, Supervision, Investigation, Data c. **Vladimir Nasluzov:** Conceptualization, Methodology, Investigation, Writing - original draft, Visualization. **Anastasia Ivaneeva:** Investigation, Visualization, Writing - original draft. **Sergey Vorobyev:** Investigation, Visualization. **Maxim Likhatski:** Investigation, Visualization, Conceptualization. **Alexander Romanchenko:** Investigation. **Alexander Krylov:** Investigation. **Sergey Zharkov:** Investigation, Visualization. **Debora Motta Meira:** Investigation, Data c.

Declaration of competing interest

The authors declare that they have no known competing financial interests or personal relationships that could have appeared to influence the work reported in this paper.

Acknowledgements

This research was supported by the Russian Foundation for Basic Research, project 18-03-00526a. We thank the ESRF for allocating beamtime, and the BM23 staff for their help during the experiments. Facilities of the Krasnoyarsk Regional Research Equipment Centre of SB RAS were employed in the work.

Appendix A. Supplementary data

Supplementary data to this article can be found online at https://doi.org/10.1016/j.matchemphys.2020.123600.

References

[1] P. Roy, S.K. Srivastava, Nanostructured copper sulfides: synthesis, properties and applications, CrystEngComm 17 (2015) 7801–7815, https://doi.org/10.1039/C5CE01304F.
[2] W. van der Stam, A.C. Berends, C. de Mello Donega, Prospects of colloidal copper chalcogenide nanocrystals, ChemPhysChem 17 (2016) 559–581, https://doi.org/10.1002/cphc.201500976.
[3] C. Coughlan, M. Ibáñez, O. Dobrozhan, A. Singh, A. Cabot, K.M. Ryan, Compound copper chalcogenide nanocrystals, Chem. Rev. 117 (2017) 5865–6109, https://doi.org/10.1021/acs.chemrev.6b00376.
[4] S. Goel, F. Chen, W. Cai, Synthesis and biomedical applications of copper sulfide nanoparticles: from sensors to theranostics, Small 10 (2014) 631–645, https://doi.org/10.1002/smll.201301174.

[5] T. Sakamoto, H. Sunamura, H. Kawaura, T. Hasegawa, T. Nakayama, M. Aono, Nanometer-scale switches using copper sulfide, Appl. Phys. Lett. 82 (2003) 3032, https://doi.org/10.1063/1.1572964.

[6] J. Xu, P. Gu, J. Zhang, H. Xue, H. Pang, Copper-based nanomaterials for high-performance lithium-ion batteries, Part. Part. Syst. Char. 33 (2016) 784–810, https://doi.org/10.1002/ppsc.201600150.

[7] K. Jiang, Z. Chen, X. Meng, CuS and Cu_2S as cathode materials for lithium batteries: a review, ChemElectroChem 6 (2019) 2825–2840, https://doi.org/10.1002/celc.201900066.

[8] S. Yadav, K. Shrivas, P.K. Bajpaia, Role of precursors in controlling the size, shape and morphology in the synthesis of copper sulfide nanoparticles and their application for fluorescence detection, J. Alloys Compnd. 772 (2019) 579–592, https://doi.org/10.1016/j.jallcom.2018.08.132.

[9] D.J. Chakrabarti, D.E. Laughlin, The Cu-S (copper-sulfur) system, Bull. Alloy Phase Diagr. 4 (1983) 254–271, https://doi.org/10.1007/BF02868665.

[10] R.J. Goble, The relationship between crystal structure, bonding and cell dimensions in the copper sulfides, Can. Mineral. 23 (1985) 61–75.

[11] H. Grijalva, M. Inoue, S. Boggavarapu, P. Calvert, Amorphous and crystalline copper sulfides, CuS, J. Mater. Chem. 6 (1996) 1157–1161, https://doi.org/10.1039/JM9960601157.

[12] D.-H. Ha, A.H. Caldwell, M.J. Ward, S. Honrao, K. Mathew, R. Hovden, M.K. A. Koker, D.A. Muller, R.G. Hennig, R.D. Robinson, Solid–solid phase transformations induced through cation exchange and strain in 2D heterostructured copper sulfide nanocrystals, Nano Lett. 14 (2014) 7090–7099, https://doi.org/10.1021/nl5035607.

[13] Y. Zhao, H. Pan, Y. Lou, X. Qiu, J. Zhu, C. Burda, Plasmonic Cu_2S nanocrystals: optical and structural properties of copper-deficient copper(I) sulfides, J. Am. Chem. Soc. 131 (2009) 4253–4261, https://doi.org/10.1021/ja805655b.

[14] J. Luther, P. Jain, T. Ewers, A.P. Alivisatos, Localized surface plasmon resonances arising from free carriers in doped quantum dots, Nat. Mater. 10 (2011) 361–366, https://doi.org/10.1038/nmat3004.

[15] Y. Xie, L. Carbone, C. Nobile, V. Grillo, S. D'Agostino, F. Della Sala, C. Giannini, D. Altamura, C. Oelsner, C. Kryschi, P.D. Cozzoli, Metallic-like stoichiometric copper sulfide nanocrystals: phase- and shape-selective synthesis, near-infrared surface plasmon resonance properties, and their modeling, ACS Nano 7 (2013) 7352–7369, https://doi.org/10.1021/nn403035s.

[16] A. Comin, L. Manna, New materials for tunable plasmonic colloidal nanocrystals, Chem. Soc. Rev. 43 (2014) 3957–3975, https://doi.org/10.1039/C3CS60265F.

[17] A. Agrawal, S.H. Cho, O. Zandi, S. Ghosh, R.W. Johns, D.J. Milliron, Localized surface plasmon resonance in semiconductor nanocrystals, Chem. Rev. 118 (2018) 3121–3207, https://doi.org/10.1021/acs.chemrev.7b00613.

[18] D. Zhu, A. Tang, L. Peng, Z. Liu, C. Yang, F. Teng, Tuning the plasmonic resonance of $Cu_{2-x}S$ nanocrystals: effects of the crystal phase, morphology and surface ligands, J. Mater. Chem. C 4 (2016) 4880–4888, https://doi.org/10.1039/C6TC00980H.

[19] Y. Xie, G. Bertoni, A. Riedinger, A. Sathya, M. Prato, S. Marras, R. Tu, T. Pellegrino, L. Manna, Nanoscale transformations in covellite (CuS) nanocrystals in the presence of divalent metal cations in a mild reducing environment, Chem. Mater. 27 (2015) 7531–7537, https://doi.org/10.1021/acs.chemmater.5b03892.

[20] K.H. Hartstein, C.K. Brozek, S.O.M. Hinterding, D.R. Gamelin, Copper-coupled electron transfer in colloidal plasmonic copper-sulfide nanocrystals probed by in situ spectroelectrochemistry, J. Am. Chem. Soc. 140 (2018) 3434–3442, https://doi.org/10.1021/jacs.8b00174.

[21] L. Chen, G. Li, Functions of 1-dodecanethiol in the synthesis and post-treatment of copper sulfide nanoparticles relevant to their photocatalytic applications, ACS Appl. Nano Mater. 1 (2018) 4587–4593, https://doi.org/10.1021/acsanm.8b00893.

[22] Z. Xu, N. Rao, C.-Y. Tang, C.-H. Cheng, W.-C. Law, Aqueous phase synthesis of $Cu_{2-x}S$ nanostructures and their photothermal generation study, ACS Omega 4 (2019) 14655–14662, https://doi.org/10.1021/acsomega.9b02204.

[23] W. van der Stam, S. Gudjonsdottir, W.H. Evers, A.J. Houtepen, Switching between plasmonic and fluorescent copper sulfide nanocrystals, J. Am. Chem. Soc. 139 (2017) 13208–13217, https://doi.org/10.1021/jacs.7b07788.

[24] S. Bhandari, S. Roy, S. Pramanik, A. Chattopadhyay, Chemical reactions involving the surface of metal chalcogenide quantum dots, Langmuir 35 (2019) 14399–14413, https://doi.org/10.1021/acs.langmuir.9b01285.

[25] Y. Xie, L. Carbone, C. Nobile, V. Grillo, S. D'Agostino, F. Della Sala, C. Giannini, D. Altamura, C. Oelsner, C. Kryschi, P.D. Cozzoli, Metallic-like stoichiometric copper sulfide nanocrystals: phase- and shape-selective synthesis, near-infrared surface plasmon resonance properties, and their modeling, ACS Nano 7 (2013) 7352–7369, https://doi.org/10.1021/nn403035s.

[26] C.H. Gammons, A.K. Frandsen, Fate and transport of metals in H_2S-rich waters at a treatment wetland, Geochem. Trans. 2 (2001) 1–15, https://doi.org/10.1186/1467-4866-2-1.

[27] K.A. Hudson-Edwards, Sources, mineralogy, chemistry and fate of heavy metal-bearing particles in mining-affected rivers systems, Mineral. Mag. 67 (2003) 205–217, https://doi.org/10.1180/0026461036720095.

[28] A.F. Hofacker, A. Voegelin, R. Kaegi, F.A. Weber, R. Kretzschmar, Temperature-dependent formation of metallic copper and metal sulfide nanoparticles during flooding of a contaminated soil, Geochem. Cosmochim. Acta 103 (2013) 316–332, https://doi.org/10.1016/j.gca.2012.10.053.

[29] K.A. Ubaid, X. Zhang, V.K. Sharma, L. Li, Fate and risk of metal sulfide nanoparticles in the environment, Environ. Chem. Lett. (2019) 1–15, https://doi.org/10.1007/s10311-019-00920-x.

[30] H. Huang, X. Zheng, S. Yang, Y. Chen, More than sulfidation: roles of biogenic sulfide in attenuating the impacts of CuO nanoparticle on antibiotic resistance genes during sludge anaerobic digestion, Water Res. 158 (2019) 1–10, https://doi.org/10.1016/j.watres.2019.04.019.

[31] R.A.D. Pattrick, J.F.W. Mosselmans, J.M. Charnock, K.E.R. England, G.R. Helz, C. D. Garner, D.J. Vaughan, The structure of amorphous copper sulfide precipitates: an X-ray absorption study, Geochem. Cosmochim. Acta 61 (1997) 2023–2036, https://doi.org/10.1016/S0016-7037(97)00061-6.

[32] Y. Mikhlin, S. Vorobyev, A. Romanchenko, S. Karasev, A. Karacharov, S. Zharkov, Ultrafine particles derived from mineral processing: a case study of the Pb-Zn sulfide ore with emphasis on lead-bearing colloids, Chemosphere 147 (2016) 60–66, https://doi.org/10.1016/j.chemosphere.2015.12.096.

[33] Y. Mikhlin, A. Romanchenko, S. Vorobyev, S. Karasev, M. Volochaev, E. Kamenskiy, E. Burdakova, Ultrafine particles in ground sulfide ores: a comparison of four Cu-Ni ores from Siberia, Russia, Ore Geol. Rev. 81 (2017) 1–9, https://doi.org/10.1016/j.oregeorev.2016.10.024.

[34] A.P. Chandra, A.R. Gerson, A review of the fundamental studies of the copper activation mechanisms for selective flotation of the sulfide minerals, sphalerite and pyrite, Adv. Colloid Interface Sci. 145 (2009) 97–110, https://doi.org/10.1016/j.cis.2008.09.001.

[35] Y. Mikhlin, S. Vorobyev, S. Saikova, Y. Tomashevich, O. Fetisova, S. Kozlova, S. Zharkov, Preparation and characterization of colloidal copper xanthate nanoparticles, New J. Chem. 40 (2016) 3059–3065, https://doi.org/10.1039/c6nj00098c.

[36] Y. Mikhlin, A. Karacharov, Y. Tomashevich, A. Shchukarev, Interaction of sphalerite with potassium n-butyl xanthate and copper sulfate solutions studied by XPS of fast-frozen samples and zeta-potential measurement, Vacuum 125 (2016) 98–105, https://doi.org/10.1016/j.vacuum.2015.12.006.

[37] F. Fu, Q. Wang, Removal of heavy metal ions from wastewaters: a review, J. Environ. Manag. 92 (2011) 407–418, https://doi.org/10.1016/j.jenvman.2010.11.011.

[38] G. Cornelis, K. Hund-Rinke, T. Kuhlbusch, N. van den Brink, C. Nickel, Fate and bioavailability of engineered nanoparticles in soils: a review, Crit. Rev. Environ. Sci. Technol. 44 (2014) 2720–2764, https://doi.org/10.1080/10643389.2013.829767.

[39] K.L. Garner, A.A. Keller, Emerging patterns for engineered nanomaterials in the environment: a review of fate and toxicity studies, J. Nanoparticle Res. 16 (2014) 2503, https://doi.org/10.1007/s1105.

[40] O. Mathon, A. Beteva, J. Borrel, D. Bugnazet, S. Gatla, R. Hino, I. Kantor, T. Mairs, M. Munoz, S. Pasternak, F. Perrin, S. Pascarelli, The time-resolved and extreme conditions XAS (Texas) facility at the European Synchrotron Radiation Facility: the general-purpose EXAFS bending-magnet beamline BM23, J. Synchrotron Radiat. 22 (2015) 1548–1554, https://doi.org/10.1107/S1600577515017786.

[41] B. Ravel, M. Newville, ATHENA, artemis, hephaestus: data analysis for X-ray absorption spectroscopy using IFEFFIT, J. Synchrotron Radiat. 12 (2005) 537–541, https://doi.org/10.1107/S0909049505012719.

[42] A. Rohrbach, J. Hafner, G. Kresse, Electronic correlation effects in transition-metal sulfides, J. Phys. Condens. Matter 15 (2003) 979–996, https://doi.org/10.1088/0953-8984/15/6/325.

[43] J.P. Perdew, J.A. Chevary, S.H. Vosko, K.A. Jackson, M.R. Pederson, D.J. Singh, C. Fiolhais, Atoms, molecules, solids, and surfaces: applications of the generalized gradient approximation for exchange and correlation, Phys. Rev. B 46 (1992) 6671–6687, https://doi.org/10.1103/PhysRevB.46.6671.

[44] J. Perdew, J. Chevary, S. Vosko, K. Jackson, M. Pederson, D. Singh, C. Fiolhais, Erratum: atoms, molecules, solids, and surfaces: applications of the generalized gradient approximation for exchange and correlation, Phys. Rev. B 48 (1993), https://doi.org/10.1103/PhysRevB.48.4978.2, 4978–4978.

[45] G. Kresse, J. Hafner, Ab initio molecular dynamics for liquid metals, Phys. Rev. B 47 (1993) 558–561, https://doi.org/10.1103/PhysRevB.47.558.

[46] G. Kresse, J. Furthmüller, Efficient iterative schemes for ab initio total-energy calculations using a plane-wave basis set, Phys. Rev. B 54 (1996) 11169–11186, https://doi.org/10.1103/PhysRevB.54.11169.

[47] S.L. Dudarev, S.Y. Savrasov, C.J. Humphreys, A.P. Sutton, Electron-energy-loss spectra and the structural stability of nickel oxide: an LSDA+U study, Phys. Rev. B 57 (1998) 1505–1509, https://doi.org/10.1103/PhysRevB.57.1505.

[48] E. Şaşıoğlu, C. Friedrich, S. Blügel, Effective Coulomb interaction in transition metals from constrained random-phase approximation, Phys. Rev. B 83 (2011) 121101, https://doi.org/10.1103/PhysRevB.83.121101.

[49] A. Morales-García, A.L. Soares, E.C. Dos Santos, H.A. de Abreu, H.A. Duarte, First-principles calculations and electron density topological analysis of covellite (CuS), J. Phys. Chem. 118 (2014) 5823–5831, https://doi.org/10.1021/jp4114706.

[50] P.E. Blöchl, Projector augmented-wave method, Phys. Rev. B 50 (1994) 17953–17979, https://doi.org/10.1103/PhysRevB.50.17953.

[51] G. Kresse, D. Joubert, From ultrasoft pseudopotentials to the projector augmented-wavemethod, Phys. Rev. B 59 (1999) 1758–1775, https://doi.org/10.1103/PhysRevB.59.1758.

[52] H.J. Monkhorst, J.D. Pack, Special points for Brillouin-zone integrations, Phys. Rev. B 13 (1976) 5188–5192, https://doi.org/10.1103/PhysRevB.13.5188.

[53] H. Fjellvåg, F. Grenvøld, S. Stølen, A.F. Andresen, R. Müller-Käfer, A. Simon, Low-temperature structural distortion in CuS, Z. für Kristallogr. - Cryst. Mater. 184 (1988) 111–121, https://doi.org/10.1524/zkri.1988.184.14.111.

[54] A. Klamt, G. Schuurmann, COSMO: a new approach to dielectric screening in solvents with explicit expressions for the screening energy and its gradient, J. Chem. Soc., Perkin Trans. 2 (1993) 799–805, https://doi.org/10.1039/P29930000799.

[55] J. Tauc, Optical properties and electronic structure of amorphous Ge and Si, Mater. Res. Bull. 3 (1968) 37–46, https://doi.org/10.1016/0025-5408(68)90023-8.

[56] A.J. Berry, A.C. Hack, J.A. Mavrogenes, M. Newville, S.R. Sutton, A XANES study of Cu speciation in high-temperature brines using synthetic fluid inclusions, Am. Mineral. 91 (2006) 1773–1782, https://doi.org/10.2138/am.2006.1940.
[57] J.R. Vegelius, K.O. Kvashnina, H. Hollmark, M. Klintenberg, Y.O. Kvashnin, I. L. Soroka, L. Werme, S.M. Butorin, X-ray spectroscopic study of Cu_2S, CuS, and copper films exposed to Na_2S solutions, J. Phys. Chem. C 116 (2012) 22293–22300, https://doi.org/10.1021/jp302390c.
[58] P. Kumar, R. Nagarajan, R. Sarangi, Quantitative X-ray absorption and emission spectroscopies: electronic structure elucidation of Cu_2S and CuS, J. Mater. Chem. C 1 (2013) 2448–2454, https://doi.org/10.1039/C3TC00639E.
[59] B.R. Tagirov, A.L. Trigub, K.O. Kvashnina, A.A. Shiryaev, D.A. Chareev, M. S. Nickolsky, V.D. Abramova, E.V. Kovalchuk, Covellite CuS as a matrix for "invisible" gold: X-ray spectroscopic study of the chemical state of Cu and Au in synthetic minerals, Geochem. Cosmochim. Acta 191 (2016) 58–69, https://doi.org/10.1016/j.gca.2016.07.015R.
[60] M. Kundu, T. Hasegawa, K. Terabe, K. Yamamoto, M. Aono, Structural studies of copper sulfide films: effect of ambient atmosphere, Sci. Technol. Adv. Mater. 9 (2008), 035011, https://doi.org/10.1088/1468-6996/9/3/035011.
[61] R. Ma, J. Stegemeier, C. Levard, J.G. Dale, C.W. Noack, T. Yang, G.E. Brown Jr., G. V. Lowry, Sulfidation of copper oxide nanoparticles and properties of resulting copper sulfide, Environ. Sci.: Nano 1 (2014) 347–357, https://doi.org/10.1039/C4EN00018H.
[62] S. Goh, A. Buckley, R. Lamb, R. Rosenberg, D. Moran, The oxidation states of copper and iron in mineral sulfides, and the oxides formed on initial exposure of chalcopyrite and bornite to air, Geochem. Cosmochim. Acta 70 (2006) 2210–2228, https://doi.org/10.1016/j.gca.2006.02.007.
[63] S. Saikova, S. Vorobyev, M. Likhatski, A. Romanchenko, S. Erenburg, S. Trubina, Y. Mikhlin, X-ray photoelectron, Cu L_3MM Auger and X-ray absorption spectroscopic studies of Cu nanoparticles produced in aqueous solutions: the effect of sample preparation techniques, Appl. Surf. Sci. 258 (2012) 8214–8221, https://doi.org/10.1016/j.apsusc.2012.05.024.
[64] M.C. Biesinger, Advanced analysis of copper X-ray photoelectron spectra, Surf. Interface Anal. 49 (2017) 1325–1334.
[65] A.L. Soares, E.C. Dos Santos, Á. Morales-García, H.A. Duarte, H.A. De Abreu, The stability and structural, electronic and topological properties of covellite (001) surfaces, Chemistry 1 (2016) 2730, https://doi.org/10.1002/slct.201600422.
[66] Z. Lv, H. Cui, H. Huang, X. Li, H. Wang, G. Ji, Study of the electronic, bonding, elastic and acoustic properties of covellite via first principles, J. Alloys Compound 692 (2017) 440–447, https://doi.org/10.1016/j.jallcom.2016.09.095.
[67] V. Nasluzov, A. Shor, A. Romanchenko, Y. Tomashevich, Y. Mikhlin, DFT+U and low-temperature XPS studies of Fe-depleted chalcopyrite ($CuFeS_2$) surfaces: a focus on polysulfide species, J. Phys. Chem. C 123 (2019) 21031–21041, https://doi.org/10.1021/acs.jpcc.9b06127.
[68] S.C. Termes, A.N. Buckley, R.D. Gillard, 2p electron binding energies for the sulfur atoms in metal polysulfides, Inorg. Chim. Acta. 126 (1987) 79–82, https://doi.org/10.1016/S0020-1693(00)81243-8.
[69] M. Fantauzzi, B. Elsener, D. Atzei, A. Rigoldi, A. Rossi, Exploiting XPS for the identification of sulfides and polysulfides, RSC Adv. 5 (2015) 75953–75963, https://doi.org/10.1039/C5RA14915K.
[70] C.G. Munce, G.K. Parker, S.A. Holt, G.A. Hope, A Raman spectroelectrochemical investigation of chemical bath deposited Cu_xS thin films and their modification, Colloid. Surface. Physicochem. Eng. Aspect. 295 (2007) 152–158, https://doi.org/10.1016/j.colsurfa.2006.08.045.
[71] M. Pal, N.R. Mathews, E. Sanchez-Mora, U. Pal, F. Paraguay-Delgado, X. Mathew, Synthesis of CuS nanoparticles by a wet chemical route and their photocatalytic activity, J. Nanoparticle Res. 17 (2015) 301, https://doi.org/10.1007/s11051-015-3103-5.
[72] I.I. Mazin, Structural and electronic properties of the two-dimensional superconductor CuS with $1^1/_3$-valent copper, Phys. Rev. B Condens. Matter 85 (2012) 115133, https://doi.org/10.1103/physrevb.85.115133.
[73] W. Liang, M.-H. Whangbo, Conductivity anisotropy and structural phase transition in covellite CuS, Solid State Commun. 85 (1993) 405–408, https://doi.org/10.1016/0038-1098(93)90689-K.
[74] N. Ghorai, H.N. Ghosh, Ultrafast plasmon dynamics and hole-phonon coupling in NIR active nonstoichiometric semiconductor plasmonic $Cu_{2-x}S$ nanocrystals, J. Phys. Chem. C 123 (2019) 28401–28410, https://doi.org/10.1021/acs.jpcc.9b10043.